J. Fluid Mech. (1997), *vol.* 334, *pp.* 353–379

The influence of entropy fluctuations on the interaction of turbulence with a shock wave

By KRISHNAN MAHESH, SANJIVA K. LELE AND PARVIZ MOIN

Center for Turbulence Research, Stanford University, Stanford, CA 94305, USA

(Received 10 June 1996 and in revised form 14 October 1996)

Direct numerical simulation and inviscid linear analysis are used to study the interaction of a normal shock wave with an isotropic turbulent field of vorticity and entropy fluctuations. The role of the upstream entropy fluctuations is emphasized. The upstream correlation between the vorticity and entropy fluctuations is shown to strongly influence the evolution of the turbulence across the shock. Negative upstream correlation between u' and T' is seen to enhance the amplification of the turbulence kinetic energy, vorticity and thermodynamic fluctuations across the shock wave. Positive upstream correlation has a suppressing effect. An explanation based on the relative effects of bulk compression and baroclinic torque is proposed, and a scaling law is derived for the evolution of vorticity fluctuations across the shock. The validity of Morkovin's hypothesis across a shock wave is examined. Linear analysis is used to suggest that shock-front oscillation would invalidate the relation between u_{rms} and T_{rms}, as expressed by the hypothesis.

1. Introduction

The interaction of shock waves with turbulent boundary layers has received considerable attention over the past five decades. There have been several experimental studies (Green 1970; Fernholz & Finley 1981; Settles & Dodson 1994; Dolling 1993) of the flow in a compression corner, normal shock/boundary layer interaction and more recently, the interaction of shock waves with three-dimensional boundary layers. These experiments testify to the complex flow field associated with the interaction. Incidence of the shock wave is shown to strongly affect both the mean flow, and the turbulent fluctuations. The Reynolds stresses and temperature fluctuations in the boundary layer are seen to amplify across the shock wave. Significant unsteadiness of the shock wave is observed when the boundary layer separates. The motion of the shock wave seems to be correlated with the upstream pressure fluctuations. Also, high levels of wall- pressure fluctuations are observed in the vicinity of the shock.

The importance of bulk compression in the evolution of the turbulence across the shock was noted by Bradshaw (1974), Dussauge & Gaviglio (1981) and Debieve, Gouin & Gaviglio (1982). Anisotropy of the upstream turbulence was identified as a significant factor by Jacquin, Blin & Geffroy (1991) and Mahesh, Lele & Moin (1993). The role of upstream acoustic waves was studied by Mahesh *et al.* (1995). By comparison, the role of entropy fluctuations in shock wave/boundary layer interaction seems to be under-appreciated. For example, Smits & Muck (1987) suggest that the primary mechanism of turbulence amplification in compression-corner flow is inviscid

bulk compression. The adverse pressure gradient, concave streamline curvature, and mean compression downstream of the corner are found to further enhance turbulence levels. Also, unsteadiness of the shock front is identified as becoming important across strong shocks.

No mention is made of the likely influence that upstream entropy fluctuations would have on the evolution of the turbulence. Morkovin's (1961) hypothesis,

$$\frac{\rho'}{\overline{\rho}} = -\frac{T'}{\overline{T}} = (\gamma - 1)M^2 \frac{u'}{U}, \tag{1.1}$$

suggests that in addition to being correlated, the intensity of the vortical field and entropy fluctuations in a constant-pressure boundary layer are of comparable magnitude. Experimental data (Bradshaw 1977) support the above hypothesis. Also, measurements (Fernholz & Finley 1981) show that $\rho_{rms}/\overline{\rho}$ in a constant-pressure boundary layer can have values as high as $5\% - 10\%$. This suggests that entropy fluctuations might play an important role in the shock wave/boundary layer interaction.

Past analytical work (Morkovin 1960; Chang 1957; Cuadra 1968) has examined the interaction of plane entropy waves with a shock. These studies emphasize the pressure field that is produced through the interaction. Morkovin's one-dimensional analysis shows that the pressure fluctuations generated behind a detached shock are quite intense, and may affect the transition of the boundary layer on the body. Cuadra's parametric study demonstrates that entropy fluctuations in shear flows can generate noise levels comparable to those generated by vortical fluctuations. Rapid distortion theory was used by Goldstein (1979) to examine the influence of upstream entropy fluctuations on turbulence passing through a wind-tunnel contraction. His analysis showed that the entropy fluctuations produced turbulence, whose magnitude increased more rapidly with contraction ratio than that of the upstream imposed turbulence. With the exception of Hesselink & Sturtevant's (1988) experiments, it appears that the interaction of a turbulent field of entropy fluctuations with a shock wave has not been examined. Also, Hesselink & Sturtevant were interested in the sonic boom problem. As a result, their study emphasized the evolution of the shock front, and restricted the shock strength to Mach 1.1.

This paper studies the interaction of a normal shock with a turbulent field of vorticity and entropy fluctuations. Direct numerical simulation (DNS) and inviscid linear analysis are used for this purpose. The focus is on the influence of the upstream entropy fluctuations. Shock waves of strength Mach 1.29 and Mach 1.8 are computed using DNS, while the linear analysis considers a range of Mach numbers from 1 to 3. The paper is organized as follows. A description of the problem is provided in §2. Some details of the DNS and linear analysis are also summarized. Section 3 discusses the results and provides an explanation for the role of entropy fluctuations. Also, a scaling law for the evolution of vorticity fluctuations across the shock is derived. The paper is then concluded with a brief summary in §4.

2. Description of the problem

Direct numerical simulation and linear analysis are used to study the interaction of a normal shock wave with turbulence. The turbulent velocity field upstream of the shock wave is isotropic, and the mean flow is uniform. Also, the upstream turbulence essentially comprises a vortical velocity field and entropic thermodynamic field. This composition is exactly enforced within the linear analysis, and is only approximately satisfied in the DNS. The upstream thermodynamic field in the DNS approximately

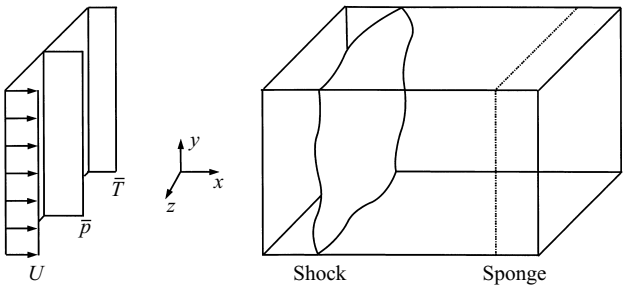

FIGURE 1. Schematic of the numerical simulation.

satisfies the weak form of Morkovin's hypothesis. The analysis considers two different spectra for the upstream thermodynamic field: one that satisfies the strong form of Morkovin's hypothesis (axisymmetric), and the other that is isotropic. Note that $\overline{u'T'}$ is negative if Morkovin's hypothesis holds upstream of the shock wave. For the isotropic upstream thermodynamic field, the analysis considers two possibilities: one where $\overline{u'T'}$ is negative, and the other where it is positive.

Section 2.1 outlines the relevant details of the DNS. The inflow and outflow boundary conditions are emphasized. A brief description of the linear analysis is then provided in §2.2.

2.1. *Details of the direct numerical simulation*

A schematic of the computed flow is shown in figure 1. Note that the shock wave is stationary in the mean. The governing equations are the unsteady three-dimensional compressible Navier–Stokes equations in the following conservative, non-dimensional form:

$$\frac{\partial \rho}{\partial t} = -\frac{\partial}{\partial x_i}(\rho u_i), \tag{2.1a}$$

$$\frac{\partial}{\partial t}(\rho u_i) = -\frac{\partial}{\partial x_j}(\rho u_i u_j + p\delta_{ij}) + \frac{\partial \tau_{ij}}{\partial x_j}, \tag{2.1b}$$

$$\frac{\partial E_t}{\partial t} = -\frac{\partial}{\partial x_i}[(E_t + p)u_i] - \frac{\partial q_i}{\partial x_i} + \frac{\partial}{\partial x_j}(u_i \tau_{ij}). \tag{2.1c}$$

The viscous stress tensor and heat flux vector are given by

$$\tau_{ij} = \frac{\mu}{Re}\left(\frac{\partial u_i}{\partial x_j} + \frac{\partial u_j}{\partial x_i} - \frac{2}{3}\frac{\partial u_k}{\partial x_k}\delta_{ij}\right), \tag{2.2a}$$

$$q_i = -\frac{\mu}{RePr}\frac{\partial T}{\partial x_i}. \tag{2.2b}$$

The variable E_t denotes the total energy, defined as $E_t = p/(\gamma-1) + \rho u_i u_i/2$. Note that the mean sound speed, density and dynamic viscosity at the inflow of the domain are used to non-dimensionalize velocity, density and viscosity respectively. The reference lengthscale L_r is related to the other reference variables by $Re = \rho_r c_r L_r/\mu_r$. The fluid is assumed to be an ideal gas with 1.4 as the ratio of specific heats. The dynamic viscosity is related to the temperature by a power law with 0.76 being the exponent, and the Prandtl number is assigned a constant value of 0.7.

The computational mesh is uniform in the directions transverse to the shock wave. A non-uniform mesh is used in the streamwise direction, such that points are clustered in the vicinity of the shock. The following analytical mapping is used for this purpose.

Using the variable s to denote a uniform mesh from 0 to 1_x, the non-uniform mesh is given by

$$\frac{x}{L_x} = \frac{rs + \dfrac{r-d}{2b} \ln\left[\dfrac{\cosh b(s-3c/2)\cosh bc/2}{\cosh b(s-c/2)\cosh 3bc/2}\right]}{r + \dfrac{r-d}{2b} \ln\left[\dfrac{\cosh b(1-3c/2)\cosh bc/2}{\cosh b(1-c/2)\cosh 3bc/2}\right]}. \tag{2.3}$$

Values of b, r, d and c used in the Mach 1.29 simulations are 12, 1.95, 0.04 and 0.281 respectively. The Mach 1.8 computation uses values of 12, 1.95, 0.02 and 0.283 respectively.

A combination of the sixth-order Padé scheme (Lele 1992) and the sixth-order ENO scheme (Shu & Osher 1988, 1989) is used to compute spatial derivatives. The shock-capturing scheme (ENO) uses the global Lax–Friedrichs flux splitting. The degeneracy in the base form of the ENO scheme is removed (Shu 1990) by biasing the adaptive choice of stencil towards central differences. Also, the shock-capturing scheme is applied only in the streamwise (shock-normal) direction in the vicinity of the shock wave. The sixth-order Padé scheme is therefore used to compute all spatial derivatives except the streamwise inviscid fluxes around the shock: the ENO scheme is used to compute those terms. Time advancement is performed using the compact-storage third-order Runge–Kutta scheme (Wray 1986). Since the turbulence is statistically homogeneous transverse to the shock wave, periodic boundary conditions are imposed in those directions. Turbulent fluctuations are superposed onto the mean field at the inflow boundary while non-reflecting boundary conditions are specified at the exit through use of a 'sponge' zone. Details of the inflow and outflow boundary conditions are provided below. The Mach 1.29 simulations are used for illustration; the same procedure was followed for the Mach 1.8 computation.

2.1.1. *Inflow turbulence*

Since the flow upstream of the shock wave is supersonic, all the flow variables are specified at the inflow boundary. Turbulent fluctuations in velocity, density and pressure are superposed on the uniform mean flow. The turbulence upstream of the shock wave is required to have an isotropic velocity field. When entropy fluctuations are present, the upstream velocity–temperature correlation is required to be similar to that found in adiabatic boundary layers, i.e. $R_{u'T'}$ is required to be nearly -1. The correlation between the velocity and temperature (entropy) fluctuations in turbulent boundary layers is a consequence of the turbulent velocity field stirring the mean temperature (entropy) gradients to produce temperature (entropy) fluctuations. However, due to the absence of a mean temperature gradient upstream of the shock in the computation, there is no mechanism to sustain a negative velocity–temperature correlation. This may be anticipated from the independence of the velocity and entropy fluctuations in the linear inviscid limit for uniform mean flow. The following procedure is therefore used to generate the desired upstream turbulence in the computations.

The turbulent fluctuations are obtained from a separate *temporal* simulation of isotropic, decaying turbulence. The temporal simulation (which has periodic boundary conditions in all three directions) is advanced in time until the flow field is well-developed, i.e. the velocity derivative skewness $S_\alpha = \overline{(\partial u'_\alpha/\partial x_\alpha)^3}/[\overline{(\partial u'_\alpha/\partial x_\alpha)^2}]^{3/2}$ attains (Tavoularis, Bennett & Corrsin 1978; Erlebacher *et al.* 1992) a value between -0.4 and -0.6. Typically, this happens after a time $t \sim \lambda/u_{rms}$. Taylor's hypothesis is then invoked, and a single realization of the developed field is convected through

the inflow plane of the spatial simulation. Details of this procedure are described by Mahesh, Lele & Moin (1996). Note that Lee, Lele & Moin (1992) have shown the validity of Taylor's hypothesis in isotropic compressible turbulence for fluctuation Mach number $M_t = (q^2)^{1/2}/\overline{c}$, and turbulence intensity $u_{rms}/\overline{U}$ as high as 0.5 and 0.15 respectively. As shown in table 1, the turbulence at the inflow is within these limits.

The simulations with the shock wave compare two different cases at each Mach number. The two cases differ in the nature of the turbulence upstream of the shock wave. While the upstream turbulence in one case (case A) is composed of vortical fluctuations, a combination of vorticity and entropy fluctuations is present in the other (case B). The upstream entropy field in case B is required to approximately satisfy the weak form of Morkovin's hypothesis, i.e. (1.1) is satisfied in the r.m.s. sense. Also, the inflow spectra and r.m.s. levels of velocity in both cases are required to essentially be the same. The same temporal simulation is therefore used to generate the inflow turbulence in the two cases.

This is done as follows. A temporal simulation of isotropic turbulence is first conducted. The initial velocity field is solenoidal with energy spectrum $E(k) \sim k^4 \mathrm{e}^{-2k^2/k_0^2}$, and the initial thermodynamic fluctuations are set to zero. The simulation is advanced in time until the velocity derivative skewness attains its developed value. An instantaneous flow field is then taken. The thermodynamic fluctuations in this field are nearly isentropic. To generate a realistic turbulent field of vorticity and entropy fluctuations, the following procedure is carried out. The pressure fluctuations in the stored flow field are set to zero while density fluctuations that satisfy $\rho'/\overline{\rho} = (\gamma - 1)M_{spat}^2 u'/U_{spat}$ are specified† (the subscript *spat* denotes spatial). This modified field is then advanced in time. Statistics from the simulation are compared to a parallel simulation, where the same field without the above modifications is advanced for the same length of time.

As expected from Kovasznay's (1955) modal decomposition, the entropy fluctuations that are introduced do not significantly influence the evolution of the velocity fluctuations. After a brief acoustic transient ($t \sim M_t \lambda/u_{rms}$), the decay rate of turbulence kinetic energy, and the velocity derivative skewness match those in the simulation without entropy fluctuations. However as expected, the solution deviates from Morkovin's hypothesis as it evolves in time. To ensure that the weak formulation of the hypothesis is approximately satisfied by the turbulence upstream of the shock, an instantaneous realization is taken immediately after the acoustic transient, and used to specify inflow turbulence in case B. A realization at exactly the same instant of time is taken from the temporal simulation without entropy fluctuations and used to specify inflow turbulence in case A.

Figures 2 and 3 present results from the temporal simulation used to generate inflow turbulence in the Mach 1.29 simulations. Note that the solution at the end of the temporal simulation is used to generate the turbulence upstream of the shock wave. The initial temporal velocity field is chosen to have fluctuation Mach number $M_t = (q^2)^{1/2}/\overline{c} = 0.22$ and microscale Reynolds number $R_\lambda = u_{rms}\lambda/\overline{\nu} = 39.5$. A uniform mesh of 81^3 points is used on a domain of length 2π in all three directions. The solution is advanced for time $t = 1.58\tau_t$, where τ_t is a turbulence time scale defined as the ratio of λ to u_{rms} at $t = 0$. As shown in figure 2, the velocity derivative skewness has attained a value of -0.48 by this time. Also, M_t and R_λ have dropped to 0.16 and 22.8 respectively. Entropy fluctuations are then introduced, and the solution

† If these entropy fluctuations were specified at $t = 0$, $R_{u'T'}$ would drop to very small levels by the time the turbulence is well-developed.

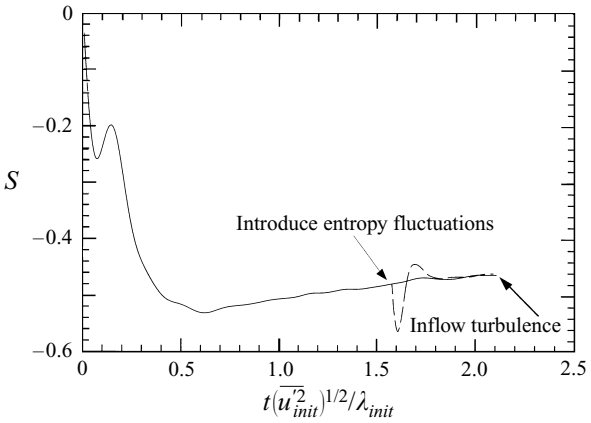

FIGURE 2. Temporal evolution of the velocity derivative skewness in the temporal decay of isotropic turbulence: ——— , without entropy fluctuations; – – – – , with entropy fluctuations.

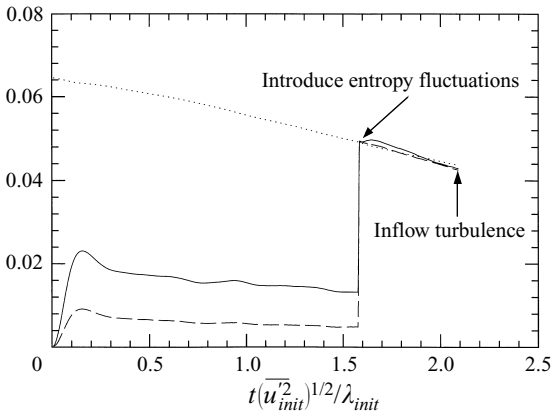

FIGURE 3. Temporal evolution of r.m.s values of terms in Morkovin's hypothesis in the temporal decay of isotropic turbulence: ——— , $\rho_{rms}/\overline{\rho}$; – – – – , $T_{rms}/\overline{T}$; ····· , $[\gamma-1]M^2_{spat}u_{rms}/U_{spat}$.

is advanced in time. At the end of the simulation, the skewness has reattained its developed value (figure 2), and the weak form of the hypothesis is approximately satisfied; $\rho_{rms}/\overline{\rho}$, $T_{rms}/\overline{T}$ and $(\gamma-1)M^2_{spat}u_{rms}/U_{spat}$ have values of 0.043, 0.043 and 0.044 respectively. By comparison, $p_{rms}/\gamma\overline{p}$ is 0.01. Also, M_t, R_λ and $\theta_{rms}/\omega_{rms}$ have values of 0.14, 20.6 and 0.085 respectively (θ_{rms} and ω_{rms} denote the r.m.s. dilatation and vorticity respectively). The solution is therefore considered to be dominated by vorticity and entropy fluctuations that approximately satisfy the weak form of Morkovin's hypothesis.

The solution at the end of the calculations shown in figures 2 and 3 is used to specify inflow turbulence in the Mach 1.29 spatial simulations. The relevant parameters of the inflow turbulence are listed in table 1. The fidelity of the temporal simulations was checked by examining the energy spectra and two-point correlations of the fluctuations. One-dimensional spectra of the velocity field show very good agreement between the two cases, A and B. The spectra show about five decades of drop-off, indicating adequate resolution. Also, two-point correlations of the velocity and density field drop off to zero, indicating adequate size of computational domain.

2.1.2. *Outflow boundary conditions*

Approximately non-reflecting boundary conditions are specified at the subsonic outflow boundary. The boundary conditions comprise a 'sponge layer' in the streamwise direction, followed by a characteristics-based boundary condition (Poinsot & Lele 1992) at the outflow plane. Boundary conditions involving a sponge layer have been used in the past in a variety of problems: e.g. Israeli & Orszag (1981), Givoli (1991), Colonius, Moin & Lele (1995). The boundary conditions with a sponge were shown to yield significantly better results than boundary conditions without the sponge layer.

The governing equations in the 'sponge layer' are modified, such that the solution in the layer is gently damped to a reference solution. A term of the form $-\sigma(\boldsymbol{U}-\boldsymbol{U}_{ref})$ is added to the right-hand side of governing equations over the sponge layer alone. $\boldsymbol{U}_{ref}$ denotes the vector of reference variables towards which the solution in the sponge layer is forced. It is obtained from the Rankine–Hugoniot equations for a laminar shock. The coefficient $\sigma(x)$ is a polynomial function; i.e.

$$\sigma(x) = A_s \frac{(x - x_s)^n}{(L_x - x_s)^n} \tag{2.4}$$

where x_s and L_x denote the start of the sponge and the length of the domain respectively. Values of A_s, n and $(L_x - x_s)/L_x$ used in our simulations are 5, 3 and 0.14 respectively.

The outflow boundary conditions are evaluated below. The interaction of the Mach 1.29 shock with a plane vorticity–entropy wave (45° incidence angle) is computed. Linear analysis predicts that the incident wave would generate downstream-propagating acoustic, vorticity and entropy waves behind the shock. The ability of the boundary conditions to allow these waves to smoothly exit the domain is thus tested. The mean flow parameters, domain length in the x-direction, and grid in the x-direction are matched to those in the turbulent simulation. The wavenumber of the upstream disturbance is set equal to the wavenumber at which the energy spectrum of the upstream turbulence peaks. The r.m.s. level of the upstream disturbance is matched to that of the upstream turbulence. The extent of the domain in y is set equal to one wavelength of the upstream disturbance, and a grid of 231 by 16 points is used to discretize the flow. The disturbance at the inflow boundary is given by the real part of (A 1*c–e*) (see the Appendix) where the variables k, ψ_1, A_v and A_e are set equal to 5, 45°, 0.05 and 0.05 respectively. The computation is initialized by a numerically computed steady laminar shock. The disturbance is then introduced at the inflow boundary. Statistics are gathered over each period of the inflow disturbance, after one domain flow-through time has passed. The statistics from successive periods are compared to check if initial transients persist. After a time $U_1 t/L_x = 3.5$, the transient effects are found negligible and the statistics have converged.

To evaluate the outflow boundary conditions, the same flow is computed on a domain twice as long behind the shock wave. 1100 points are used in the streamwise direction. The resulting resolution is greater than that in the shorter domain. Statistics from the two simulations are then compared to each other and to linear analysis. Figure 4 shows the streamwise evolution of the averaged kinetic energy, vorticity and density in the two computations. Only the 'useful region' $(L_x - x_s)$ of the shorter domain is shown. Good agreement between the two computations is observed, indicating that the non-reflecting nature of the sponge region is acceptable. Some influence of the sponge region (maximum value about 3.5%) on the statistics of $\overline{v'^2}$ and $\overline{\rho'^2}$ is observed immediately upstream of the sponge.

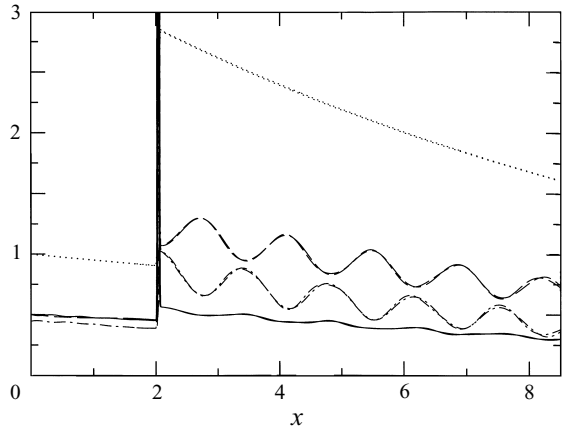

FIGURE 4. Spatial evolution of statistics from a computation of the interaction of a Mach 1.29 shock wave with a plane vorticity–entropy wave. Results from short and long domains are both indicated as follows: ——— , $\overline{u'^2}/q_{in}^2$; - - - - , $\overline{v'^2}/q_{in}^2$; ····· , $\overline{\omega'^2}/\overline{\omega_{in}'^2}$; — - — , $(\overline{\rho'^2}/\overline{\rho_2}^2)/(q_{in}^2/U_1^2)$. The subscript *in* denotes inflow.

The spatial evolution of the statistics is not compared to inviscid linear analysis owing to significant viscous decay in the computation. However, the amplification of statistics immediately across the shock wave is compared to analysis. The comparison shows that the error (computed with respect to analysis) in $\overline{u'^2}, \overline{v'^2}, \overline{\omega'^2}$ and $\overline{\rho'^2}$ is $0.8\%, 1.6\%, 0.8\%$ and 0.5% respectively. Linear analysis shows that only waves whose incidence angle is less than a critical incidence angle generate downstream-propagating disturbances behind the shock. Evanescent waves are generated at higher angles of incidence. In computing shock/turbulence interaction, the fraction of incident waves that generate these downstream-propagating disturbances poses the primary challenge to outflow boundary conditions. The performance of the outflow boundary for the incidence angle of 45° suggests that the boundary conditions are quite adequate for the turbulent simulations.

In evaluating the outflow boundary conditions, it was mentioned that the streamwise grid was the same as that used in the turbulent simulation. This streamwise grid is chosen as follows. The shock-capturing scheme is used to compute the corresponding steady laminar shock, and the solution is evaluated. The ENO schemes are known (Meadows, Caughy & Casper 1993; Woodward & Collela 1984; Roberts 1990; Lindquist & Giles 1991) to produce spurious entropy oscillations when applied to slowly moving shock waves. In contrast to standard central differences, these oscillations are bounded; they do not cause instability. The spurious oscillations in density and temperature are typically the largest, those in velocity and pressure are much smaller. To compute shock/turbulence interaction, we require that the amplitude of these spurious oscillations be small compared to the physical fluctuations. The amplitude of these spurious oscillations can be reduced by increasing the shock speed relative to the mesh (Meadows *et al.* 1993), or by refining the mesh (for a viscous computation). The shock is stationary in the mean in our computations. The shock speed with respect to the grid is therefore determined entirely by the upstream disturbances. We therefore use the shock-capturing scheme to compute the corresponding laminar shock, and refine the mesh until the spurious oscillations are acceptably small. For example, the mesh used in our Mach 1.29 computations yields

spurious density oscillations that are 0.03% of the mean density behind the Mach 1.29 shock (the spurious oscillations in temperature, velocity and pressure are smaller). Table 1 shows that the upstream intensity of density fluctuations in the turbulent simulations is greater than 1.2%. The above level of spurious oscillations generated by the shock-capturing scheme is therefore considered acceptable. This streamwise grid is then used to perform the computations.

2.1.3. *Simulations performed*

The relevant parameters of the numerical simulations are given in table 1. Note that the values at the inflow are quoted. Essentially, the simulations consider the interaction of low-Reynolds-number turbulence with shock waves of strengths equal to Mach 1.29 and Mach 1.8. Note that one of the cases (free-stream Mach number 2.9, wedge angle 8°) in the compression-corner experiments of Smits & Muck (1987) yields a normal Mach number of 1.29 if one assumes that the entire flow is turned across a single shock. Also, only one simulation (with upstream entropy fluctuations) is performed for the Mach 1.8 shock. In §2.1 it was noted that the shock-capturing scheme was only applied in the streamwise direction for the Mach 1.29 shock wave. However, applying the shock-capturing scheme in only the streamwise direction set up unstable oscillations for the Mach 1.8 shock. As a result, the shock-capturing scheme was applied in all three directions in the immediate vicinity of the shock for the Mach 1.8 shock wave.

2.2. *Linear analysis*

Details of the linear analysis are provided in the Appendix. Essentially, the linearized Euler equations are used to study the interaction between the upstream turbulence and the shock wave, which is modelled as a discontinuity. The upstream turbulence (being homogeneous) is represented as a superposition of Fourier modes (plane waves), each of which independently interacts with the shock. The analysis is therefore initiated by considering the interaction of a single plane wave with the shock. Workers such as Ribner (1953, 1954) and Chang (1957) have developed the procedure to obtain the disturbance field behind the shock and the distortion of the shock front. Other references to work using linear analysis are provided by Mahesh *et al.* (1995). This solution is then integrated over all the incident waves to obtain a statistical description of the turbulence behind the shock wave. The turbulence statistics thus obtained are functions of the distance behind the shock wave, the Mach number of the shock, and the incident velocity and density spectra. In presenting results from the linear analysis, this paper will occasionally refer to the variables A_r and ϕ_r. Essentially, A_r represents the amplitude of the upstream density field, and ϕ_r represents the sign of the upstream velocity–temperature correlation. If $\phi_r = 0$, $\overline{u'T'}$ is negative upstream of the shock wave; $\phi_r = 180°$ implies that $\overline{u'T'}$ is positive upstream of the shock.

3. Results

Turbulence statistics in the simulation are computed by averaging over time and the y- and z-directions. The ratios of mean velocity, temperature and pressure across the shock wave are very nearly equal to their corresponding laminar values (Mahesh *et al.* 1996). A small overshoot in pressure and temperature is observed immediately downstream of the shock. The mean velocity exhibits a corresponding

	Case 1.29A	Case 1.29B	Case 1.8
M_1	1.29	1.29	1.8
R_λ	19.1	19.1	19.5
M_t	0.14	0.14	0.18
$(q^2)^{1/2}/\overline{U_1}$	0.11	0.11	0.10
$\rho_{rms}/\overline{\rho_1}$	0.012	0.042	0.076
$T_{rms}/\overline{T_1}$	0.0042	0.041	0.076
$p_{rms}/\gamma\overline{p_1}$	0.011	0.010	0.018
$\overline{u'T'}/u_{rms}T_{rms}$	−0.06	−0.84	−0.85
(N_x, N_y, N_z)	(231, 81, 81)	(231, 81, 81)	(231, 81, 81)

TABLE 1. Parameters in the simulations performed.

undershoot, following which it remains practically constant. However, mean pressure and temperature exhibit a small positive gradient behind the shock wave. The presence of upstream entropy fluctuations has no noticeable effect on the mean flow behind the shock. Entropy fluctuations do however influence the thickness of the shock wave as inferred from the mean flow profiles. The 'mean shock thickness' is larger in the presence of entropy fluctuations; i.e. the mean gradients in the vicinity of the shock are smaller. Given that the 'mean shock thickness' reflects the amplitude of shock oscillation, this indicates an increase in shock motion when the upstream fluctuations satisfy Morkovin's hypothesis.

The following sections present results for the evolution of the turbulence across the shock. The results from the DNS and linear analysis are compared. In §3.1 the evolution of the turbulence kinetic energy across the shock are discussed. The influence of the shock on the vorticity fluctuations is considered in §3.2. This is followed in §3.3 by a physical argument for the role of the upstream entropy fluctuations. In §3.4 a scaling for the amount of vorticity produced by the upstream entropy fluctuations is derived. Then in §3.5 the evolution of the thermodynamic fluctuations and the validity of Morkovin's hypothesis across the shock are discussed.

3.1. *Turbulence kinetic energy*

The presence of upstream entropy fluctuations has a noticeable effect on the evolution of turbulence kinetic energy across the shock wave. Figures 5 and 6 show the streamwise evolution of turbulence kinetic energy in cases 1.29A and 1.29B. Note that $\overline{v'^2} = \overline{w'^2}$ behind the shock. The intermittency associated with shock oscillation is seen to cause high fluctuation levels in the vicinity of the shock (Debieve & Lacharme 1986; Lee *et al.* 1992). The width of this intermittent region (denoted by δ_{inter}) nearly equals the 'mean shock thickness'. Using the mean velocity profile to determine its value, $k_0\delta_{inter}$ is approximately 0.3 and 0.4 in cases 1.29A and 1.29B respectively† . We focus our attention on the evolution of kinetic energy outside this intermittent region in the following paragraphs.

As shown in figure 6, kinetic energy levels behind the shock wave are noticeably higher in case 1.29B. The streamwise component is affected more than the transverse components. Comparison of the peak in the profile of $\overline{u'^2}$ (at $k_0x = 14$) reveals 20% higher levels in case 1.29B. Comparison of $\overline{v'^2}$ at the same location shows

† The smallest mesh spacing is in the vicinity of the shock, and is equal to $0.02/k_0$ in both simulations. Also, the shock-capturing scheme is applied over a width equal to $1.8/k_0$ on either side of the mean shock.

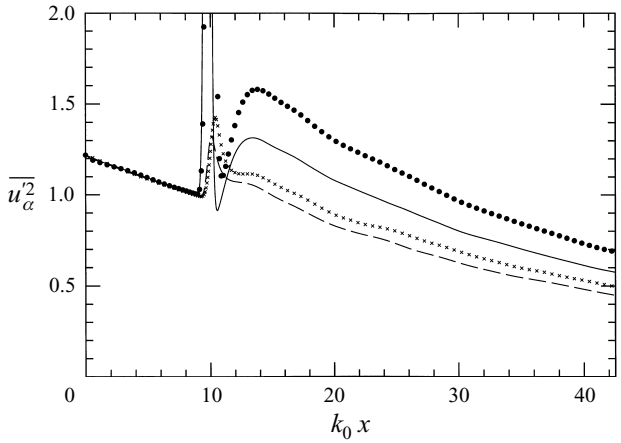

FIGURE 5. Turbulence kinetic energy from DNS of the Mach 1.29 shock wave. All the curves are normalized by their value immediately upstream of the shock ($k_0 x = 8.97$): ——— , $\overline{u'^2}$, case 1.29A; – – – – , $\overline{v'^2}$, case 1.29A; • , $\overline{u'^2}$, case 1.29B; × , $\overline{v'^2}$, case 1.29B.

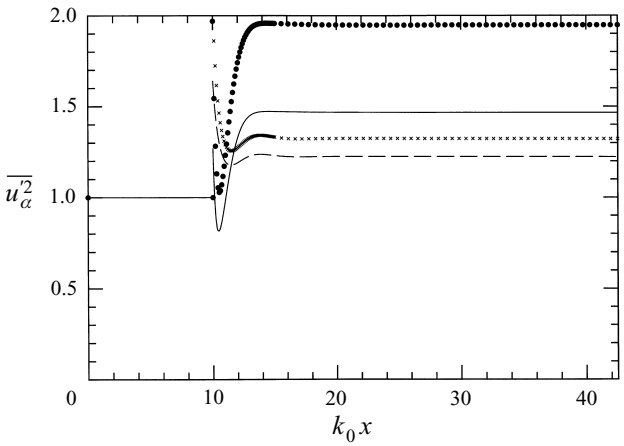

FIGURE 6. Evolution of turbulence kinetic energy behind a Mach 1.29 shock wave as predicted by linear analysis. All the curves are normalized by their value immediately upstream of the shock: ——— , $\overline{u'^2}$, without entropy fluctuations; – – – – , $\overline{v'^2}$, without entropy fluctuations; • , $\overline{u'^2}$, with entropy fluctuations; × , $\overline{v'^2}$, with entropy fluctuations.

the level of enhancement to be a modest 7%. This enhancement in the presence of entropy fluctuations is predicted by linear analysis. Note that quantitative comparison of turbulence kinetic energy between analysis and DNS is made difficult by the viscous decay in the simulations. If the peak levels of kinetic energy behind the shock wave are compared, the linear analysis predictions are seen to be higher. As seen from figure 6, the amplification of $\overline{u'^2}$ as predicted by linear analysis is 1.47 and 1.95 in the absence and presence of entropy fluctuations (that satisfy Morkovin's hypothesis) respectively. Corresponding values for $\overline{v'^2}$ are predicted to be 1.22 and 1.32 respectively. Thus linear analysis predicts that the upstream entropy fluctuations would enhance the amplification of $\overline{u'^2}$ by 33%, and that of $\overline{v'^2}$ by about 8%.

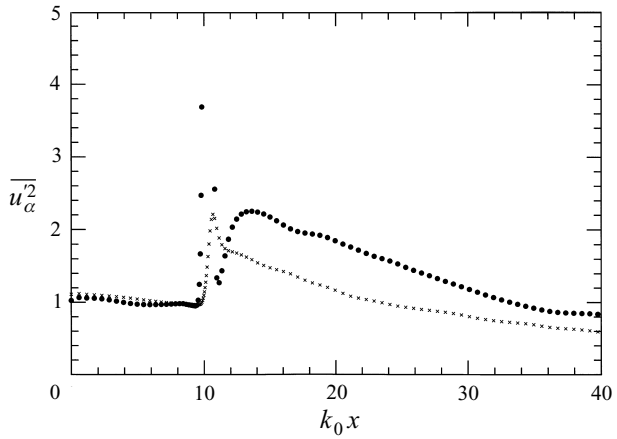

FIGURE 7. Turbulence kinetic energy from DNS of the Mach 1.8 shock wave. Both the curves are normalized by their value immediately upstream of the shock. • , $\overline{u'^2}$; × , $\overline{v'^2}$.

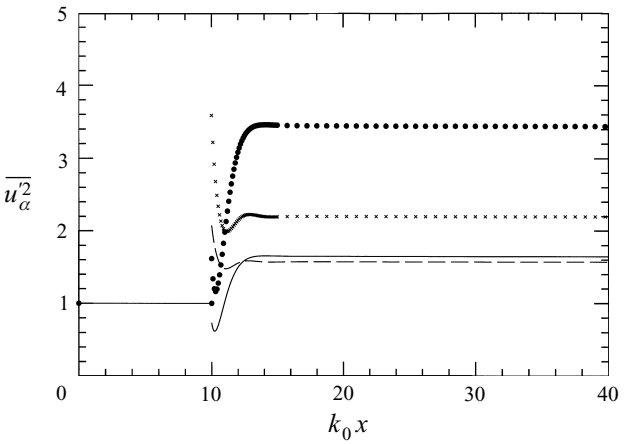

FIGURE 8. Evolution of turbulence kinetic energy behind a Mach 1.8 shock wave as predicted by linear analysis. All the curves are normalized by their value immediately upstream of the shock: ——— , $\overline{u'^2}$, without entropy fluctuations; – – – – , $\overline{v'^2}$, without entropy fluctuations; • , $\overline{u'^2}$, with entropy fluctuations; × , $\overline{v'^2}$, with entropy fluctuations.

Figures 7 and 8 show the evolution of turbulence kinetic energy across the Mach 1.8 shock wave. The amplification levels are noticeably higher than those across the Mach 1.29 shock. Using values measured at $k_0 x = 13.4$ (the location behind the shock where $\overline{u'^2}$ is maximum) $\overline{u'^2}$ and $\overline{v'^2}$ are seen to amplify by 2.25 and 1.61 respectively. These levels are lower than predicted by linear analysis, where Morkovin's hypothesis is assumed to exactly hold upstream of the shock. The predicted (far-field) values of kinetic energy amplification are 3.44 and 2.2 respectively. Linear analysis predicts that the upstream entropy fluctuations would enhance the amplification of $\overline{u'^2}$ and $\overline{v'^2}$ by 110% and 40% respectively across a Mach 1.8 shock.

Note that $\overline{u'T'}$ is negative if Morkovin's hypothesis is valid. Linear analysis shows that the sign of the correlation between the upstream velocity and entropy fields is of considerable importance. If the upstream correlation between u' and

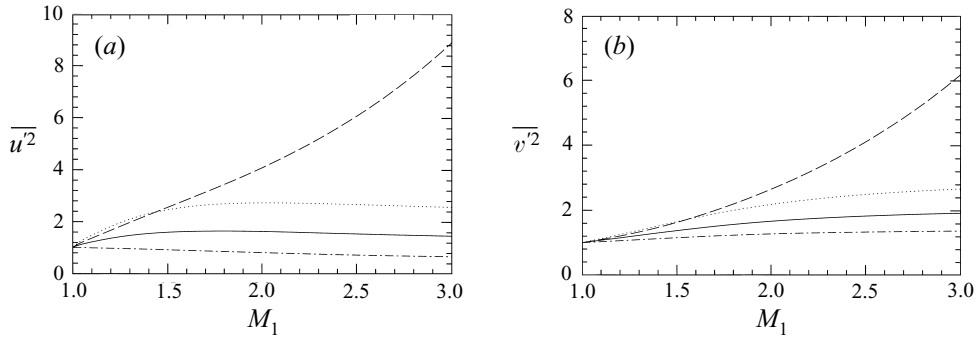

FIGURE 9. (*a*) $\overline{u'^2}$ and (*b*) $\overline{v'^2}$ in the far field of the shock wave as predicted by linear analysis. All the curves are normalized by their upstream values. ——— , pure vorticity; – – – – , Morkovin's hypothesis satisfied upstream; ····· , $A_r = 0.54, \phi_r = 0°$; — – — , $A_r = 0.54, \phi_r = 180°$.

T' is negative, then the upstream entropy fluctuations are seen to enhance kinetic energy amplification. This is the trend seen in the DNS. However, if $\overline{u'T'}$ is positive upstream of the shock, the amplification of kinetic energy is strongly suppressed. Practical situations where this might occur include strongly cooled boundary layers, and mixing layers where the mean velocity and density gradients are of opposite sign. This influence of entropy fluctuations increases with increasing Mach number. Figures 9(*a*) and 9(*b*) show linear analysis predictions of kinetic energy amplification in the far field of the shock wave. If Morkovin's hypothesis is assumed to hold upstream, the amplification of $\overline{u'^2}$ is predicted to be enhanced by more than 100% for Mach numbers exceeding about 1.8. The primary reason for this increase in enhancement with increasing Mach number is that $(\rho_{rms}/\overline{\rho})/(q_{rms}/U)$ increases with Mach number if Morkovin's hypothesis is satisfied upstream of the shock wave.

3.2. *Vorticity fluctuations*

All components of vorticity are affected by the upstream entropy fluctuations. As shown in figure 10(*a*), the levels of vorticity fluctuations behind the shock wave are higher in case 1.29B. The amplification of $\overline{\omega_2'^2}$ is seen to increase by 8.7% when entropy fluctuations are present upstream of the shock. This increase is qualitatively predicted by linear analysis. The increase in amplification predicted by analysis is much higher – about 19.4%. The primary reason for this difference between analysis and DNS is believed to be the strict imposition of Morkovin's hypothesis upstream of the shock in the analysis. Owing to the absence of mean temperature gradients, the upstream fluctuations in the simulation only approximately satisfy Morkovin's hypothesis (table 1). Support for this reasoning is provided by the fact that the vorticity amplification in case 1.29A is within 6.3% of analysis while the deviation in case 1.29B is about 16.2%.

Linear analysis predicts the transverse vorticity components to amplify across the shock wave, and remain constant downstream. The streamwise vorticity component is predicted to remain constant across and downstream of the shock. DNS shows that the streamwise vorticity component does indeed remain constant across the shock. However, it increases immediately downstream of the shock wave. In fact, the peak level of $\overline{\omega_1'^2}$ behind the shock wave in case 1.29B is about 7.1% greater than its upstream value. Lee *et al.* (1992) noted for vortical upstream turbulence that this behaviour is nonlinear in nature; it is caused by the stretching of vorticity fluctuations

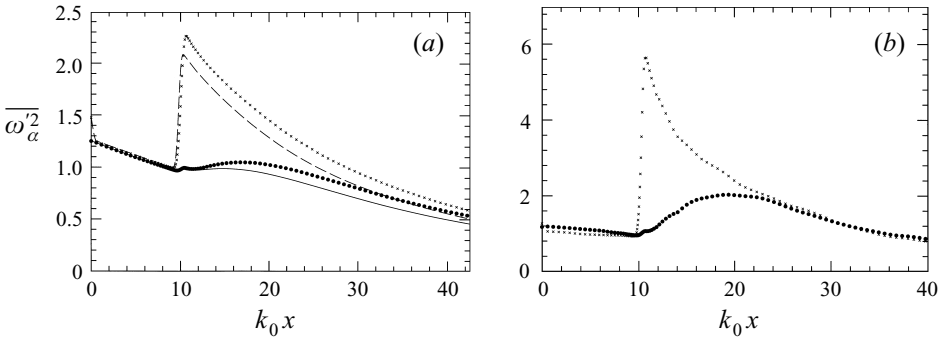

FIGURE 10. Streamwise evolution of vorticity fluctuations from DNS of (*a*) the Mach 1.29 shock wave and (*b*) the Mach 1.8 shock wave. All the curves are normalized by their value immediately upstream of the shock ($k_0 x = 8.97$). (*a*) ——— , $\overline{\omega_1'^2}$, case 1.29A; – – – – , $\overline{\omega_2'^2}$, case 1.29A; • , $\overline{\omega_1'^2}$, case 1.29B; × , $\overline{\omega_2'^2}$, case 1.29B. (*b*) • , $\overline{\omega_1'^2}$; × , $\overline{\omega_2'^2}$.

by the fluctuating strain rate. In the presence of upstream entropy fluctuations, it is likely that nonlinear baroclinic effects might provide an additional contribution. This downstream rise in $\overline{\omega_1'^2}$ is noticeably higher behind the Mach 1.8 shock. As shown in figure 10(*b*), the peak level of $\overline{\omega_1'^2}$ behind the Mach 1.8 shock is about twice its upstream value. By comparison, Lee *et al.*'s results (in the absence of upstream entropy fluctuations) show that $\overline{\omega_1'^2}$ behind a Mach 2 shock is about 1.5 times its upstream value. The inability to predict this rise in $\overline{\omega_1'^2}$ behind the shock wave is probably the most serious limitation of the linear analysis. Also, it is interesting to note (figures 7 and 10(*b*)) that the vorticity fluctuations in the DNS approach isotropy more rapidly than the velocity fluctuations. This is consistent with the notion that the small scales would return to isotropy more rapidly than the larger scales. Linear analysis is used to determine the influence of mean Mach number on the amplification of the transverse vorticity fluctuations in figure 11. As observed with the turbulence kinetic energy, negative upstream $\overline{u'T'}$ is seen to enhance the amplification of vorticity fluctuations, while positive correlation is seen to suppress it.

3.3. *A simple explanation*

An explanation is provided here for the influence of entropy fluctuations on the evolution of a turbulent flow across a shock wave. Note that Hayes' (1957) results (equation (30) in his paper) for the jump in vorticity across an unsteady shock wave require the unsteady evolution of the shock front to be known accurately enough that derivatives normal and tangent to the front may be obtained. This is quite difficult to obtain from a computation where the shock wave is 'captured' in the Navier–Stokes equations. It is therefore not possible to use Hayes' results to interpret the DNS. Consider the following idealization of the mean field associated with the shock:

$$U = U(x), \quad \overline{p} = \overline{p}(x), \quad \overline{\rho} = \overline{\rho}(x). \tag{3.1}$$

Linearizing the Euler equations about the above mean flow yields the following governing equations for the vorticity fluctuations (denoted by ω'):

$$\omega_t' + U\omega_x' = -\omega' U_x - \frac{\rho_y'}{\overline{\rho}^2}\,\overline{p}_x + \frac{p_y'}{\overline{\rho}^2}\,\overline{\rho}_x. \tag{3.2}$$

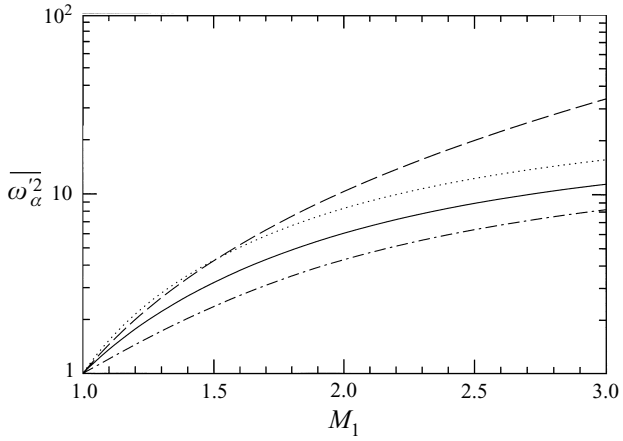

FIGURE 11. Amplification of $\overline{\omega_2'^2} = \overline{\omega_3'^2}$ across the shock wave as predicted by linear analysis. ———, Pure vorticity; – – – –, Morkovin's hypothesis satisfied upstream; ·····, $A_r = 0.54, \phi_r = 0°$; — – —, $A_r = 0.54, \phi_r = 180°$.

Note that although irrotational acoustic fluctuations are generated at the shock, their contribution to the downstream kinetic energy is not significant; linear analysis (Mahesh *et al.* 1996) shows that vortical fluctuations account for about 99% of the turbulence kinetic energy behind the shock wave. Equation (3.2) represents the effects of bulk change on the evolution of vorticity fluctuations across the shock. Linear effects due to shock distortion are absent. Also, the effects of shock curvature (Hayes 1957) are ignored. As a result of these assumptions, the relations obtained are expected to function more as scaling laws than predictive formulae.

If the incident disturbance comprises vorticity and entropy fluctuations, then $p' = 0$ in the incident field and hence

$$\omega_t' + U\omega_x' = -\omega' \, U_x - \frac{\rho_y'}{\overline{\rho}^2} \, \overline{p}_x. \tag{3.3}$$

The term $-\omega' U_x$ represents the effect of bulk compression. The drop in mean velocity across the shock wave indicates that this term would enhance the incident vorticity fluctuations. The incident entropy fluctuations produce vorticity at the shock wave through the baroclinic term. The baroclinic contribution can enhance or oppose the effect of bulk compression. The phase difference between the upstream vorticity and entropy waves determines whether enhancement or opposition is observed.

Consider for example the plane vorticity–entropy wave represented by (A 1*c–e*). It is easily shown that

$$-\omega' U_x - \frac{\rho_y'}{\overline{\rho}^2} \, \overline{p}_x \sim A_v \, U U_x - A_e \, l \frac{\overline{p}_x}{\overline{\rho}}. \tag{3.4}$$

Since U_x is negative and $\overline{p}_x$ is positive across a shock wave, the two sources of vorticity are of the same sign if A_e and A_v are of the same sign. They oppose each other if A_e and A_v are of opposite sign. Thus if u' and T' are negatively correlated, the entropy field enhances the amplification of fluctuating vorticity. On the other hand, a positive correlation between u' and T' suppresses the amplification of vorticity across the shock wave.

Further insight is gained from a schematic illustration of this effect. Figure 12 shows

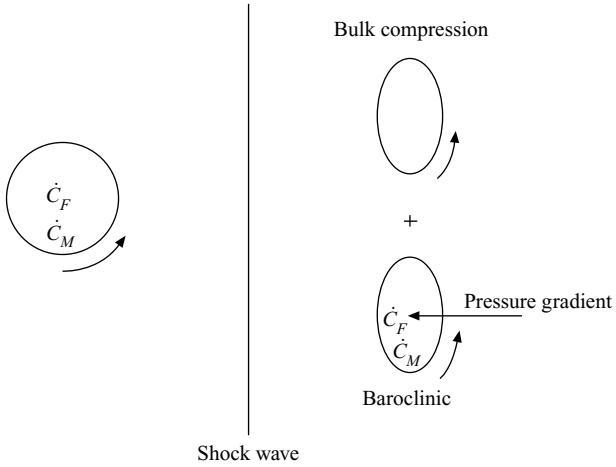

FIGURE 12. A spherical element of fluid passing through a shock wave. The effects of bulk compression and baroclinic vorticity production are shown. u' and T' are negatively correlated upstream of the shock wave.

a fluid element of circular cross-section passing through a shock wave. The geometric centre of this element is denoted by C_F, while C_M denotes the centre of mass. The disturbance field associated with the fluid element is that of a vorticity–entropy wave. The element therefore exhibits solid-body rotation (with associated vorticity ω') which is assumed positive in the direction shown. Also, the density gradient associated with the entropy wave causes the centre of mass to differ from the centre of force (the geometric centre). Note that C_M is below C_F if the correlation between u' and T' is negative. Bulk compression compresses the element in the streamwise direction thereby enhancing the rotation. In addition, the shock wave exerts a pressure force (associated with the adverse pressure gradient) that passes through C_F. This pressure force would exert a torque about the centre of mass. This torque manifests itself as the baroclinic source of vorticity. Note that if C_M is below C_F the baroclinic rotation is in the same direction as the rotation due to bulk compression. It is in the opposite direction if C_M is above C_F (positive correlation between u' and T'). The upstream correlation between u' and T' thus determines the location of C_M with respect to C_F, and thereby the relative sense of rotation that the baroclinic torque produces.

3.4. *Scaling of the evolution of vorticity across a shock wave*

Equation (3.3) is used to derive approximate expressions for the evolution of vorticity fluctuations across the shock. The expressions are evaluated by comparing to the linear analysis predictions. Equation (3.3) is rewritten as

$$\mathrm{D}_t(U\omega') = -\frac{\rho'_y}{\overline{\rho}^2}\, U\overline{p}_x \tag{3.5}$$

where D_t denotes the material derivative $\partial/\partial t + U\partial/\partial x$. Using the relation $\overline{p}_x = -\overline{\rho}UU_x$ in the above equation yields

$$\mathrm{D}_t(U\omega') = \frac{\rho'_y}{\overline{\rho}}\, U^2U_x = \frac{\rho'_y}{3\overline{\rho}}\, (U^3)_x. \tag{3.6}$$

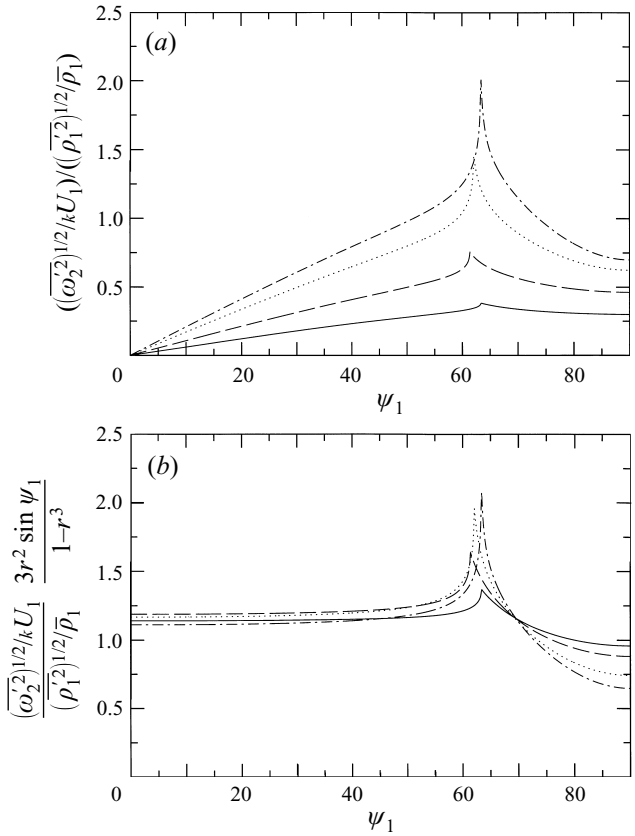

FIGURE 13. (*a*) Unscaled and (*b*) scaled r.m.s. vorticity produced in the interaction of an entropy wave with a shock wave. ——— ($M_1 = 1.25$), – – – – ($M_1 = 1.5$), ····· ($M_1 = 2$), — – — ($M_1 = 2.5$).

The shock wave is approximated as a discontinuity. $(U^3)_x$ is expressed as $\Delta(U^3)\delta(x)$, where $\Delta(U^3)$ represents the difference in U^3 across the shock wave, and $\delta(x)$ denotes the Dirac delta function. An approximate solution to the above equation is obtained by setting ρ_y' equal to its upstream value (see (A 1*c–e*)). Transforming coordinates to $x' = x - Ut, \tau = t$ and integrating yields the following expression for the change in vorticity across the shock wave:

$$U_2\omega_2' - U_1\omega_1' \sim \frac{\mathrm{i}kl}{3}A_e\frac{U_2^3 - U_1^3}{U_1}, \tag{3.7}$$

which yields

$$\omega_2' \sim r\omega_1' + \frac{\mathrm{i}kl}{3}\ A_e\ U_1\ \frac{1-r^3}{r^2} \tag{3.8}$$

where $r = U_1/U_2$ is obtained from the Rankine–Hugoniot equations. Equation (3.8) suggests that incident vorticity fluctuations amplify by an amount equal to the mean density ratio. The vorticity produced by the incident entropy fluctuations is predicted to scale as $kA_e \sin\psi_1(1-r^3)/r^2$.

These expressions are next compared to linear analysis. Figures 13(*a*) and 13(*b*) show the levels of vorticity produced when an entropy wave interacts with a shock. Mean Mach numbers from 1.25 to 2.5 are considered. Both unscaled and scaled

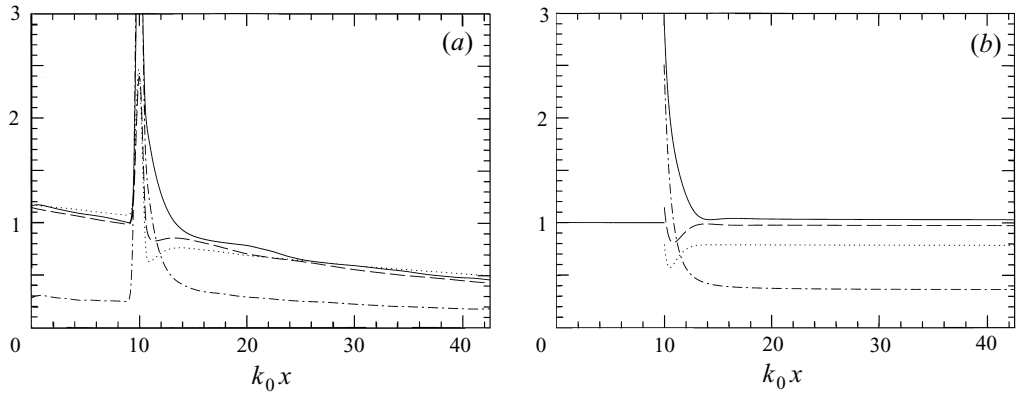

FIGURE 14. The intensities of thermodynamic fluctuations (*a*) from DNS and (*b*) as predicted by linear analysis, for case 1.29B. All variables are non- dimensionalized by the value of $\rho_{rms}/\overline{\rho}$ immediately upstream of the shock wave ($k_0x = 8.97$). ——— , $\rho_{rms}/\overline{\rho}$; - - - - , $T_{rms}/\overline{T}$, ····· , $(\gamma-1)M^2u_{rms}/U$; —·— , $p_{rms}/\gamma\overline{p}$.

values of r.m.s. vorticity behind the shock wave are plotted as a function of incidence angle. The proposed scaling seems to yield reasonable collapse of the curves in the propagating regime. The validity of the scaling for a turbulent field would depend upon the fraction of incident waves in the propagating regime.

The interaction of a vorticity wave with a shock has been considered, and the scaling compared to linear analysis (Mahesh *et al.* 1996). The scaling was less satisfactory: unscaled values ranging from 1 to 6 were collapsed to vary from 0.5 to 1.4. The amplification of incident vorticity was very nearly equal to the mean density ratio for incidence angles near zero; however, a systematic deviation was seen with increasing incidence angle. This evolution of the vorticity waves is in agreement with Jacquin, Cambon & Blin (1993) who observe large discrepancies at the higher Mach numbers when the effect of shock distortion is not represented in the linear limit.

3.5. *Thermodynamic fluctuations and Morkovin's hypothesis*

The thermodynamic fluctuations behind weak shock waves were noted by Lee, Lele & Moin (1994) to be nearly isentropic. The thermodynamic field in case 1.29A follows this trend, i.e. $p_{rms}/\gamma\overline{p}$, $\rho_{rms}/\overline{\rho}$ and $T_{rms}/(\gamma-1)\overline{T}$ are nearly equal over the entire domain. However, upstream entropy fluctuations were not present in Lee *et al.*'s computations. As might be expected, the downstream thermodynamic field is not isentropic when upstream entropy fluctuations are present. Figure 14(*a*) shows the streamwise evolution of the pressure, density and temperature fluctuations in case 1.29B. The quantity $(\gamma-1)M^2u_{rms}/U$ is also shown. This allows the weak form of Morkovin's hypothesis to be evaluated across the shock. The corresponding predictions made by linear analysis are shown in figure 14(*b*).

Good qualitative agreement is observed between analysis and simulation. The intensity of pressure fluctuations in the near field is seen to be comparable to that of the density and temperature. However, the pressure fluctuations decay behind the shock wave, causing their far-field intensity to be smaller. Considerable deviation from Morkovin's hypothesis is observed in the near field behind the shock. The extent of deviation in the far field is seen to be smaller. The linear analysis predicts a larger deviation from the hypothesis in the far field than the DNS. Owing to viscous decay, the notion of far field is not as precise in the DNS as it is in the analysis. Linear

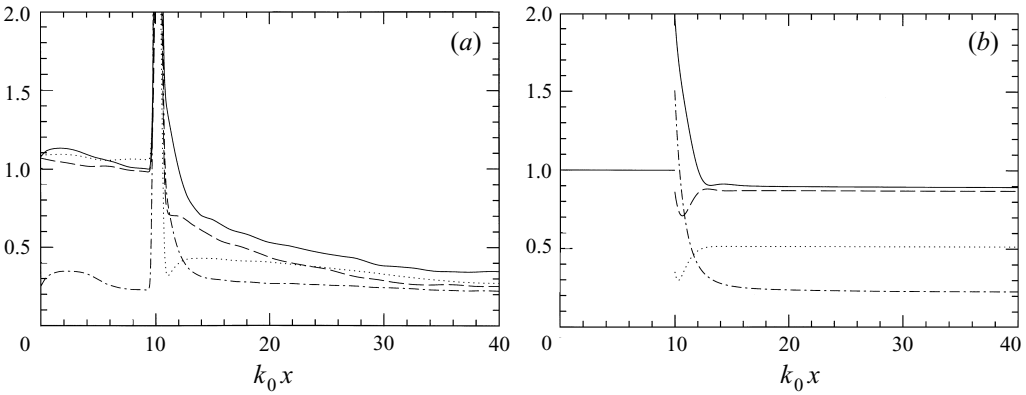

FIGURE 15. Thermodynamic fluctuations (*a*) from DNS and (*b*) as predicted by linear analysis, for case 1.8. All variables are non-dimensionalized by the value of $\rho_{rms}/\overline{\rho}$ immediately upstream of the shock wave. ——— , $\rho_{rms}/\overline{\rho}$; - - - - , $T_{rms}/\overline{T}$, ····· , $(\gamma-1)M^2u_{rms}/U$; —·— , $p_{rms}/\gamma\overline{p}$.

analysis suggests (figure 14(*b*)) that the far-field values are attained at approximately $k_0x = 17$. If the weak form of Morkovin's hypothesis is evaluated at this location in the computation, it shows behaviour comparable to analysis. Interestingly however, the validity of the hypothesis in the DNS is seen to increase with distance downstream of this location. The exact cause of this trend is not known. Also, although the r.m.s values of the terms in the hypothesis approach each other behind the shock in the DNS, $\overline{u'T'}/u_{rms}T_{rms}$ does not approach -1. It drops in magnitude across the shock, and decreases further in magnitude downstream, e.g. the correlation coefficient at $k_0x = 20$ is -0.54.

A similar trend is observed in the Mach 1.8 computation. Morkovin's hypothesis is evaluated across the Mach 1.8 shock wave in figures 15(*a*) and 15(*b*) respectively. The far-field values in the analysis are attained at about $k_0x = 15$. Both analysis and DNS show considerable deviation from the hypothesis at this location. However, the intensities of the density and temperature fluctuations decay behind the shock wave in the DNS, resulting in increased validity of the hypothesis behind the shock. Interestingly, although $\rho_{rms}/\overline{\rho}$, $T_{rms}/\overline{T}$ and $(\gamma-1)M^2u_{rms}/U$ approach each other behind the shock, the intensity of the pressure fluctuations is not negligible. As seen in figure 15(*a*), $p_{rms}/\gamma\overline{p}$ is nearly of the same magnitude as $T_{rms}/\overline{T}$ at about $k_0x = 40$. Also, $\overline{u'T'}/u_{\rm rms}T_{rms}$ does not approach -1. Its value at $k_0x = 20$ is -0.22.

Linear analysis is used to examine the influence of mean Mach number on the validity of Morkovin's hypothesis across the shock wave. The incident fluctuations are constrained to satisfy the strict form of the hypothesis. The fluctuations in the far field are then examined to see if the hypothesis holds in the r.m.s. sense. The results (figure 16) show that the first part of the hypothesis, i.e. $\rho_{rms}/\overline{\rho} = T_{rms}/\overline{T}$, is still a good approximation behind the shock wave (especially if M_1 is less than about 2). However, the part of the hypothesis that relates T' to u' exhibits large deviation with Mach number. This behaviour is explained below.

The equation $\rho'/\overline{\rho} = -T'/\overline{T}$ is obtained by setting p' to zero in the linearized equation of state. It amounts to neglecting the acoustic mode in comparison to the entropy mode. As seen from (*A*1*d*), it holds exactly for the upstream turbulence. Upon interaction with the shock, the incident fields of vorticity and entropy fluctuations generate acoustic waves. The generation of acoustic waves is however accompanied by amplification of the incident entropy fluctuations. Also, a fraction of

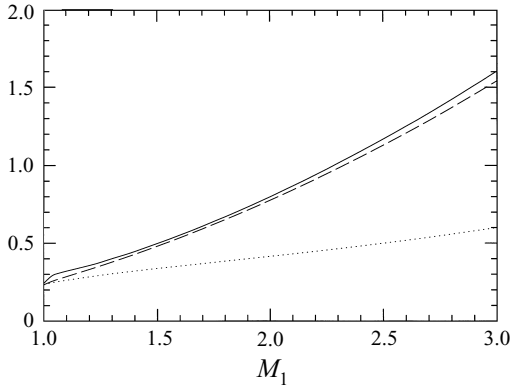

FIGURE 16. Evaluation of Morkovin's hypothesis in the far field of the shock wave using linear analysis. All the curves are non-dimensionalized by the upstream value of u_{rms}/U. ——— , $\rho_{rms}/\overline{\rho}$; – – – – , $T_{rms}/\overline{T}$; ····· , $(\gamma-1)M^2 u_{rms}/U$.

the acoustic waves decays behind the shock. As a result, the acoustic contribution to the thermodynamic fluctuations in the far field is significant only at the larger Mach numbers. The first part of the weak form of Morkovin's hypothesis is therefore a good approximation behind shock waves of moderate strength.

The relation

$$\frac{T'}{\overline{T}} = -(\gamma-1)M^2\frac{u'}{U} \tag{3.9}$$

is obtained by assuming that stagnation temperature fluctuations are small in the linear limit. Denote the stagnation temperature by T_0,

$$T_0 = \overline{T} + T' + \frac{(U+u')^2 + v'^2 + w'^2}{2C_p}, \tag{3.10}$$

where C_p denotes the specific heat at constant pressure. Linearizing the above equation yields the following expression for fluctuations in stagnation temperature: $T_0' = T' + Uu'/C_p$. Setting T_0' to zero and rearranging yields (3.9).

In the linear limit, fluctuations in stagnation temperature obey the relation, $\mathrm{D}T_0'/\mathrm{D}t = \partial p'/\partial t$ behind the shock wave ($\mathrm{D}/\mathrm{D}t$ denotes the material derivative based on the mean velocity). Decomposing the temperature field into acoustic and entropic components, and the velocity into acoustic and vortical components allows decomposition of T_0' into T_{0ent}' and T_{0acous}' such that $\mathrm{D}T_{0ent}'/\mathrm{D}t = 0$ and $\mathrm{D}T_{0acous}'/\mathrm{D}t = \partial p'/\partial t$. Next, the Rankine–Hugoniot equations may be used to show that (3.9) cannot be valid behind a shock wave if it is assumed to hold upstream of the shock. The energy equation requires the stagnation temperature to be constant across the shock in a frame of reference that moves at the instantaneous speed of the shock wave, i.e.

$$\overline{T}_1 + T_1' + \frac{(U_1+u_1'-\xi_t)^2 + v_1'^2 + w_1'^2}{2C_p} = \overline{T}_2 + T_2' + \frac{(U_2+u_2'-\xi_t)^2 + v_2'^2 + w_2'^2}{2C_p}. \tag{3.11}$$

Linearizing the above equation and constraining the incident fluctuations to satisfy (3.9) yields

$$T_2' + \frac{U_2 u_2'}{C_p} = -\frac{\xi_t}{C_p}(U_1 - U_2), \tag{3.12}$$

i.e. the fluctuations of stagnation temperature are not zero immediately behind the

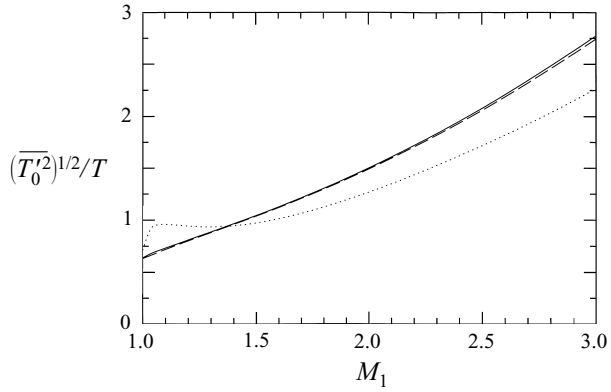

FIGURE 17. Decomposition of stagnation temperature fluctuations using linear analysis. All the curves are non-dimensionalized by the upstream value of u_{rms}/U. ——— , Far-field value; – – – – , contribution due to vorticity and entropy fluctuations; ····· , near-field value.

shock wave. Dividing through by $\overline{T}_2$ and rearranging, we get

$$\frac{T_2'}{\overline{T}_2} + (\gamma - 1)M_2^2 \frac{u_2'}{U_2} = -(\gamma - 1)M_2 \left(\frac{U_1}{U_2} - 1 \right) \frac{\xi_t}{a_2}. \tag{3.13}$$

Thus, applicability of Morkovin's hypothesis immediately behind the shock wave requires that

$$(\gamma - 1)M_2 \left(\frac{U_1}{U_2} - 1 \right) \frac{\xi_t}{a_2} \quad \sim \quad 0. \tag{3.14}$$

The r.m.s. values of the near-field ($k_0 x = 10$) stagnation temperature are plotted in figure 17 as a function of the mean Mach number. The plotted values are seen to be comparable to the terms in Morkovin's hypothesis (figure 16). The hypothesis is therefore invalid immediately behind the shock wave. The above argument is next extended to show why the hypothesis does not hold in the far field. Decomposition of the stagnation temperature fluctuations into vorticity–entropy and acoustic components shows that both near- and far-field values of the stagnation temperature fluctuations are dominated by the vorticity–entropy component. As shown in figure 17, the vorticity–entropy component is nearly equal to the total level in the far field, while its contribution to the near-field level is greater than 80% over the range of Mach numbers shown. Figure 17 and (3.13) therefore show that appreciable levels of stagnation temperature fluctuations are generated immediately behind the shock wave due to oscillation of the shock front. Most of these fluctuations arise from vorticity–entropy fluctuations, which convect downstream to generate an appreciable level of stagnation temperature fluctuations in the far field of the shock wave. This leads to inapplicability of Morkovin's hypothesis in the far field.

4. Summary

Direct numerical simulation and inviscid linear analysis were used to study the interaction of a normal shock wave with an isotropic turbulent field of vorticity and entropy fluctuations. Shock waves of strength Mach 1.29 and Mach 1.8 were computed using DNS, while the linear analysis considered a range of Mach numbers from 1 to 3. Our objective was to study the role of the upstream entropy fluctuations in the evolution of the turbulent flow across the shock.

The upstream entropy fluctuations were shown to significantly affect shock/turbulence interaction. The magnitude of the entropy fluctuations, and the sign of the upstream velocity–temperature correlation were both seen to be important. Higher levels of kinetic energy and vorticity amplification were observed across the shock when u' and T' were negatively correlated upstream of the shock. Positive correlation had the opposite effect. An explanation was provided to explain these trends. The evolution of fluctuating vorticity across the shock wave was noted to have two important contributions: bulk compression of incident vorticity and baroclinic production of vorticity through the incident entropy fluctuations. The upstream correlation between vorticity and entropy fluctuations was shown to determine whether these two sources of vorticity enhance or oppose each other, thereby determining kinetic energy levels behind the shock wave. A scaling was then proposed for the evolution of vorticity across the shock wave. Since Morkovin's hypothesis is known to apply in adiabatic turbulent boundary layers, the results suggest that the entropy fluctuations in the boundary layer would play a very significant role in the interaction between the boundary layer and a shock wave.

The validity of Morkovin's hypothesis behind a shock was examined. Linear analysis indicates that neglecting the acoustic mode is a good approximation in the far field of shock waves of moderate strength ($M_1 < 2$). The part of the hypothesis relating u' and T' was predicted to be invalid. Non-negligible oscillation of the shock front was shown to be responsible. The thermodynamic fluctuations in the simulations followed linear analysis predictions immediately behind the shock. Interestingly however, the terms in the weak form of the hypothesis approached each other as the solution decayed behind the shock. Despite this trend, the pressure fluctuations in the DNS were not negligible in the far field. Also, $\overline{u'T'}$ did not approach -1. Its value in the far field was about -0.54 and -0.22 for the Mach 1.29 and Mach 1.8 shock waves.

This study was supported by the Air Force Office of Scientific Research under Grant 88-NA-322 and Contract F49620-92-J-0128 with Dr Leonidas Sakell as the technical monitor. The authors would also like to express their gratitude to NAS and NASA-Ames Research Center for the use of their computer facilities.

Appendix

The linear analysis is summarized below. The interaction of a single vorticity–entropy wave with a shock is first considered in §A.1. The analysis is then extended in §A.2 to describe the evolution of the turbulent field across the shock.

A.1. *Interaction of a shock with a plane vorticity–entropy wave*

The two-dimensional interaction of a shock wave with a plane vorticity–entropy wave is schematically illustrated in figure 18. Note that the shock wave is stationary in the mean. The variables $U, \overline{p}, \overline{\rho}, \overline{T}$ and M denote the mean velocity, pressure, density, temperature and Mach number respectively and subscripts 1 and 2 denote the upstream and downstream states. The flow upstream of the shock wave is perturbed by the weak disturbance field of the incident vorticity–entropy wave which is assumed to be a plane wave that makes angle ψ_1 with the x-axis. The variables u', v', p', ρ' and T' represent the fluctuating velocities, pressure, density and temperature. The

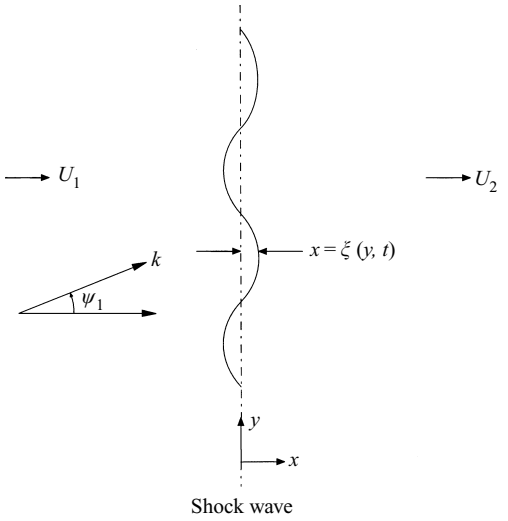

FIGURE 18. Schematic of the interaction of a vorticity–entropy wave with a shock wave.

incident field has the following form:

$$\frac{u_1'}{U_1} = lA_v\ \mathrm{e}^{\mathrm{i}k(mx+ly-U_1mt)}, \quad \frac{v_1'}{U_1} = -mA_v\ \mathrm{e}^{\mathrm{i}k(mx+ly-U_1mt)}, \tag{A 1a,b}$$

$$\frac{\rho_1'}{\overline{\rho}_1} = A_e\ \mathrm{e}^{\mathrm{i}k(mx+ly-U_1mt)}, \quad \frac{T_1'}{\overline{T}_1} = -\frac{\rho_1'}{\overline{\rho}_1}, \quad p_1' = 0, \tag{A 1c–e}$$

where $m = \cos\psi_1$ and $l = \sin\psi_1$. The shock wave deforms in response to the incident disturbance; the displacement is denoted by $x = \xi(y, t)$.

Details of the analysis may be found in Mahesh *et al.* (1996). The solution obtained is summarized below. The solution behind the shock wave is a superposition of vortical, acoustic and entropic components. It has the following dimensionless form:

$$\frac{1}{A_v}\frac{u_2'}{U_1} = \widetilde{F}\ \mathrm{e}^{\mathrm{i}\widetilde{k}x}\mathrm{e}^{\mathrm{i}k(ly-mU_1t)} + \widetilde{G}\ \mathrm{e}^{ik(mrx+ly-mU_1t)}, \tag{A 2a}$$

$$\frac{1}{A_v}\frac{v_2'}{U_1} = \widetilde{H}\ \mathrm{e}^{\mathrm{i}\widetilde{k}x}\mathrm{e}^{\mathrm{i}k(ly-mU_1t)} + \widetilde{I}\ \mathrm{e}^{\mathrm{i}k(mrx+ly-mU_1t)}, \tag{A 2b}$$

$$\frac{1}{A_v}\frac{p_2'}{\overline{p}_2} = \widetilde{K}\ \mathrm{e}^{\mathrm{i}\widetilde{k}x}\mathrm{e}^{\mathrm{i}k(ly-mU_1t)}, \tag{A 2c}$$

$$\frac{1}{A_v}\frac{\rho_2'}{\overline{\rho}_2} = \frac{\widetilde{K}}{\gamma}\ \mathrm{e}^{\mathrm{i}\widetilde{k}x}\mathrm{e}^{\mathrm{i}k(ly-mU_1t)} + \widetilde{Q}\ \mathrm{e}^{\mathrm{i}k(mrx+ly-mU_1t)}, \tag{A 2d}$$

$$\frac{1}{A_v}\frac{T_2'}{\overline{T}_2} = \frac{\gamma-1}{\gamma}\widetilde{K}\ \mathrm{e}^{\mathrm{i}\widetilde{k}x}\mathrm{e}^{\mathrm{i}k(ly-mU_1t)} - \widetilde{Q}\ \mathrm{e}^{\mathrm{i}k(mrx+ly-mU_1t)}. \tag{A 2e}$$

The boundary conditions across the shock wave yield the following expressions for the velocity and slope of the shock front:

$$\frac{1}{A_v}\frac{\xi_t}{U_1} = \widetilde{L}\ \mathrm{e}^{\mathrm{i}k\ (ly-mU_1t)}, \quad \frac{1}{A_v}\xi_y = -\frac{l}{m}\widetilde{L}\ \mathrm{e}^{\mathrm{i}k\ (ly-mU_1t)}. \tag{A 3}$$

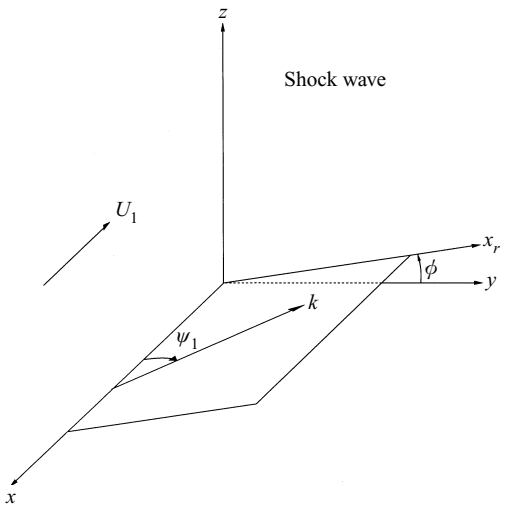

FIGURE 19. Coordinate system used in the interaction of isotropic turbulence with a shock wave.

The variable r denotes the mean density ratio $\overline{\rho}_2/\overline{\rho}_1$ across the shock wave; $\widetilde{k}(M_1, \psi_1)$ represents the streamwise wavenumber of the acoustic component behind the shock wave. It is real in the propagating regime and complex in the decaying regime. The coefficients $\widetilde{F}, \widetilde{H}$ and $\widetilde{K}$ are associated with the acoustic component. The vortical component is represented by $\widetilde{G}$ and $\widetilde{I}$ while $\widetilde{Q}$ represents the entropy component. The coefficients $\widetilde{F}, \widetilde{H}$, $\widetilde{K}, \widetilde{G}$, $\widetilde{I}$ and $\widetilde{Q}$ are functions of M_1, ψ_1 and the amplitude ratio (A_r) and phase difference (ϕ_r) between the vorticity and entropy waves, i.e. $A_r e^{i\phi_r} = A_e/A_v$. Expressions for the coefficients are given in Mahesh *et al.* (1996).

A.2. *Interaction of a shock wave with an isotropic turbulent field*

As suggested by Morkovin's hypothesis, the upstream turbulence is represented as a random three-dimensional field of vorticity–entropy waves. The turbulent velocity field is assumed to be isotropic. The incident turbulent field is represented as a superposition of plane vorticity–entropy waves (Fourier modes) in three dimensions. Each of these waves would interact independently with the shock wave under linear analysis. For a given upstream spectrum, the interaction of each wave with the shock wave is predicted. The solution is integrated over all incident waves to obtain turbulence statistics behind the shock.

The three-dimensional problem is related to the two-dimensional analysis of the preceding section as follows. Consider an incident plane wave in three dimensions. As shown in figure 19, the wavenumber vector of the wave lies in a plane that makes angle ϕ with the y-axis. In this plane, which we call the (x, x_r)-plane, the wave makes angle ψ_1 with the x-axis. It is readily seen that the (x, x_r)-plane is identical to the plane of interaction in the two-dimensional problem. The solenoidal nature of the incident velocity field requires the velocity vector of the wave to be normal to the wavenumber vector. The velocity field may therefore be expressed as a sum of two components: one normal to the wavenumber vector in the (x, x_r)-plane and the other normal to the (x, x_r)-plane (the ϕ-direction). It is intuitively clear that the ϕ-component of velocity would pass unchanged through the shock wave. As a result, the three-dimensional problem may be solved using results of the two-dimensional analysis in the (x, x_r)-plane.

Results from §A.1 are used to obtain expressions for the energy spectra behind the shock wave. The spectra depend upon the upstream three-dimensional energy spectrum, $E(k)$. This paper assumes the following form for $E(k)$:

$$E(k) \sim \left(\frac{k}{k_0}\right)^4 \mathrm{e}^{-2(k/k_0)^2}. \tag{A 4}$$

The results also depend upon the upstream density spectrum. The quantity A_e/A_v may be represented as $A_r \mathrm{e}^{\mathrm{i}\phi_r}$, where A_r and ϕ_r are both functions of the wavenumber vector. Appropriate functional dependencies may be assumed depending upon the flow being considered. This paper presents results for $\phi_r = 0$ and π, i.e. the density field is either perfectly correlated or perfectly anti-correlated with the velocity field, Also, two forms of the upstream density spectrum are considered. One case assumes the density field to be isotropic with the same three-dimensional spectrum as the velocity field, i.e. A_r is assumed constant. For this case it is easily shown that

$$A_r = \sqrt{2}\frac{(\overline{\rho_1'^2})^{1/2}/\overline{\rho_1}}{(q_1^2)^{1/2}/U_1}. \tag{A 5}$$

The second case assumes that the density field satisfies Morkovin's hypothesis at every wavenumber. If the velocity fluctuations are isotropic, it is easily seen that the resulting density field is axisymmetric, i.e.

$$A_r = (\gamma - 1)M^2 \sin\psi_1. \tag{A 6}$$

The spectra are then numerically integrated to obtain the turbulence statistics behind the shock. Further details are provided by Mahesh *et al.* (1996).

REFERENCES

Bradshaw, P. 1974 The effect of mean compression or dilatation on the turbulence structure of supersonic boundary layers. *J. Fluid Mech.* **63**, 449–464.

Bradshaw, P. 1977 Compressible turbulent shear layers. *Ann. Rev. Fluid Mech.* **9**, 33–54.

Chang, C. T. 1957 Interaction of a plane shock and oblique plane disturbances with special reference to entropy waves. *J. Aero. Sci.* **24**, 675–682.

Colonius, T., Moin, P. & Lele, S. K. 1995 Direct computation of aerodynamic sound. *Rep. TF-65.* Department of Mechanical Engineering, Stanford University, Stanford, California.

Cuadra, E. 1968 Flow perturbations generated by a shock wave interacting with an entropy wave. *AFOSR-UTIAS Symp. on Aerodynamic Noise, Toronto*, pp. 251–271. University of Toronto Press.

Debieve, F. R., Gouin, H. & Gaviglio, J. 1982 Evolution of the Reynolds stress tensor in a shock wave-turbulence interaction. *Indian J. Technol.* **20**, 90–97.

Debieve, J. F. & Lacharme, J. P. 1986 A shock wave/free-turbulence interaction. In *Turbulent Shear Layer/Shock Wave Interactions* (ed. J. Delery). Springer.

Dolling, D. S. 1993 Fluctuating loads in shock wave/turbulent boundary layer interaction: tutorial and update. *AIAA Paper* 93-0284.

Dussauge, J. P. & Gaviglio, J. 1987 The rapid expansion of a supersonic turbulent flow: role of bulk dilatation. *J. Fluid Mech.* **174**, 81–112.

Erlebacher, G., Hussaini, M. Y., Speziale, C. G. & Zang, T. A. 1992 Towards the large eddy simulation of compressible turbulent flows. *J. Fluid Mech.* **238**, 155–185.

Fernholz, H. H. & Finley, P. J. 1981 A further compilation of compressible boundary layer data with a survey of turbulence data. *AGARDograph* 263.

Givoli, D. 1991 Non-reflecting boundary conditions. *J. Comput. Phys.* **94**, 1–29.

Goldstein, M. E. 1979 Turbulence generated by the interaction of entropy fluctuations with non-uniform mean flows. *J. Fluid Mech.* **93**, 209–224.

Green, J. E. 1970 Interaction between shock waves and turbulent boundary layers. *Prog. Aerospace Sci.* **11**, 235–340.

Hayes, W. D. 1957 The vorticity jump across a gasdynamic discontinuity. *J. Fluid Mech.* **2**, 595–600.

Hesselink, L. & Sturtevant, B. 1988 Propagation of weak shocks through a random medium. *J. Fluid Mech.* **196**, 513–553.

Honkan, A. & Andreopoulous, J. 1992 Rapid compression of grid-generated turbulence by a moving shock wave. *Phys. Fluids* A **4**, 2562–2572.

Israeli, M. & Orszag, S. A. 1981 Approximation of radiation boundary conditions. *J. Comput. Phys.* **41**, 115–135.

Jacquin, L., Blin, E. & Geffroy, P. 1991 Experiments on free turbulence/shock wave interaction. *Proc. Eighth Symp. on Turbulent Shear Flows, Munich* (ed. F. Durst, R. Friedrich, B. E. Launder, F. W. Schmidt, U. Schumann & J. H. Whitelaw). Springer.

Jacquin, L., Cambon, C. & Blin, E. 1993 Turbulence amplification by a shock wave and rapid distortion theory. *Phys. Fluids* A **5**, 2539–2550.

Keller, J. & Merzkirch, W. 1990 Interaction of a normal shock wave with a compressible turbulent flow. *Exps. Fluids* **8**, 241–248.

Kovasznay, L. S. G. 1953 Turbulence in supersonic flow. *J. Aero. Sci.* **20**, 657–682.

Lee, S., Lele, S. K. & Moin, P. 1992 Simulation of spatially evolving turbulence and the applicability of Taylor's hypothesis in compressible flow. *Phys. Fluids* A **4**, 1521–1530.

Lee, S., Lele, S. K. & Moin, P. 1993 Direct numerical simulation of isotropic turbulence interacting with a weak shock wave. *J. Fluid Mech.* **251**, 533–562. Also see Corrigendum, *J. Fluid Mech.* **264**, 373–374.

Lee, S., Lele, S. K. & Moin, P. 1994 Interaction of isotropic turbulence with a strong shock wave. *AIAA Paper* 94-0311.

Lele, S. K. 1992 Compact finite difference schemes with spectral-like resolution. *J. Comput. Phys.* **103**, 16–42.

Lele, S. K. 1994 Compressibility effects on turbulence. *Ann. Rev. Fluid Mech.* **26**, 211–254.

Lindquist, D. R. & Giles, M. B. 1991 On the validity of linearized unsteady Euler equations with shock-capturing. *AIAA Paper* 91-1598-CP.

Mahesh, K., Lee, S., Lele, S. K. & Moin, P. 1995 The interaction of an isotropic field of acoustic waves with a shock wave *J. Fluid Mech.* **300**, 383–407.

Mahesh, K., Lele, S. K. & Moin, P. 1993 The response of anisotropic turbulence to rapid homogeneous one-dimensional compression. *Phys. Fluids* **6**, 1052–1062.

Mahesh, K., Lele, S. K. & Moin, P. 1996 The interaction of a shock wave with a turbulent shear flow. *Report* TF-69. Thermosciences Division, Mechanical Engineering Department, Stanford University, Stanford, CA.

Meadows, K. R., Caughey, D. A. & Casper, J. 1993 Computing unsteady shock waves for aeroacoustic applications. *AIAA Paper* 93-4329.

Morkovin, M. V. 1960 Note on the assessment of flow disturbances at a blunt body traveling at supersonic speeds owing to flow disturbances in the free stream. *Trans. ASME. J. Appl. Mech.*, No. 60-APM-10.

Morkovin, M. V. 1961 Effects of compressibility on turbulent flows. In *Mecanique de la Turbulence* (ed. A. Favrè), pp. 367–380. Paris, Editions du Centre National de la Recherche Scientifique.

Poinsot, T. J. & Lele, S. K. 1992 Boundary conditions for direct simulation of compressible viscous reacting flow. *J. Comput. Phys.* **101**, 104–129.

Ribner, H. S. 1953 Convection of a pattern of vorticity through a shock wave. *NACA TN* 2864.

Ribner, H. S. 1954 Shock-turbulence interaction and the generation of noise. *NACA TN* 3255.

Roberts, T. W. 1990 The behavior of flux difference splitting schemes near slowly moving shocks. *J. Comput. Phys.* **90**, 141–160.

Settles, G. S. & Dodson, L. J. 1994 Supersonic and hypersonic shock/boundary-layer interaction database. *AIAA J.* **32**, 1377–1383.

Shu, C.-W. 1990 Numerical experiments on the accuracy of ENO and modified ENO schemes. *J. Sci. Comput.* **5**, 127–149.

Shu, C.-W. & Osher, S. 1988 Efficient implementation of essentially non-oscillatory shock-capturing schemes. *J. Comput. Phys.* **77**, 439–471.

Shu, C.-W. & Osher, S. 1989 Efficient implementation of essentially non-oscillatory shock-capturing schemes II. *J. Comput. Phys.* **83**, 32–78.

Smits, A. J. & Muck, K. C. 1987 Experimental study of three shock wave/turbulent boundary layer interactions. *J. Fluid Mech.* **182**, 294–314.

Tavoularis, S., Bennett, J. C. & Corrsin, S. 1978 Velocity-derivative skewness in small Reynolds number, nearly isotropic turbulence. *J. Fluid Mech.* **176**, 33–66.

Woodward, P. & Collela, P. 1984 The numerical simulation of two-dimensional flow through shocks. *J. Comput. Phys.* **54**, 115–173.

Wray, A. A. 1986 Very low storage time-advancement schemes. *Internal Rep.* NASA-Ames Research Center, Moffett Field, CA.